A sparse EEG-informed fMRI model for hybrid EEG-fMRI neurofeedback prediction

Claire Cury[1,2], Pierre Maurel[1], Rémi Gribonval[2], and Christian Barillot[1]

[1] Univ Rennes, CNRS, Inria, Inserm, IRISA UMR 6074, Empenn ERL U 1228, F-35000 Rennes, France.
[2] Univ Rennes, CNRS, Inria, IRISA UMR 6074, PANAMA team, F-35000 Rennes, France.

Abstract. Measures of brain activity through functional magnetic resonance imaging (fMRI) or Electroencephalography (EEG), two complementary modalities, are ground solutions in the context of neurofeedback (NF) mechanisms for brain-rehabilitation protocols. Though NF-EEG (real-time neurofeedback scores computed from EEG) have been explored for a very long time, NF-fMRI (real-time neurofeedback scores computed from fMRI) appeared more recently and provides more robust results and more specific brain training. Using simultaneously fMRI and EEG for multimodal neurofeedback sessions (NF-EEG-fMRI, real-time neurofeedback scores computed from fMRI and EEG) is very promising to devise brain rehabilitation protocols. However using fMRI is costly, exhausting and time consuming, and cannot be repeated too many times for the same subject. The original contribution of this paper concerns the prediction of multimodal NF scores from EEG recordings only, using a training phase where both EEG and fMRI synchronous signals, and therefore neurofeedback scores, are available. We propose a sparse regression model able to exploit EEG only to predict NF-fMRI or NF-EEG-fMRI in motor imagery tasks. We compare different NF-predictors steming from the proposed model. We show that one of the proposed NF-predictors significanlty improves over what EEG can provide alone (without the learning phase), and correlates at 0.74 in median with the ground-truth.

Keywords: Optimisation, EEG, fMRI, sparsity, learning, NFB

1 Introduction

Neurofeedback approaches (NF) are non-invasive measurements of brain activity (usually based on only one modality) [11,27] through online brain functional feature extraction, to provide real-time feedback to a subject about its brain activity and help him or her perform a given task. NF appears to be an interesting approach for clinical purposes, for example in the context of rehabilitation and psychiatric disorders [27,4,30]. Functional magnetic resonance imaging (fMRI) and electro-encephalography (EEG) are the most used noninvasive functional brain imaging modalities in neurofeedback.

EEG measures the electrical activity of the brain through channels located on the scalp. EEG has an excellent temporal resolution (milliseconds), but a limited spatial resolution. Besides, EEG is not easy to control in neurofeedback for the subject or patient, since it directly comes from mixtures of propagating electric potential fluctuations, measured on the scalp, providing noisy data.

On the other hand, blood oxygenation level dependent (BOLD) fMRI, measures a delayed hemodynamic response to neural activity with a good spatial resolution, and a temporal resolution of 1 or 2 seconds depending on the sequence used. In addition it is easier to control the hemodynamics of the brain activity, which is more stable and less noisy than electrical activity, making the fMRI an adequate modality for neurofeedback (NF-fMRI) [29]. However this is a costly, exhausting for subjects and time consuming modality, and unfortunately, NF-fMRI cannot be repeated too many times for the same subject.

During the past few years, the use of simultaneous EEG-fMRI recording has been used to understand the links between EEG and fMRI in different states of the brain activity and received recognition as a promising multi-modal measurement of the brain activity [23,1]. Since this bi-modal acquisition is still not comfortable for subjects or patients, it is costly and not portable, due to the use of fMRI. Therefore, the methodology to extract information from fMRI with EEG have been also intensively investigated (some methods involved in the process are reviewed here [1]). Indeed, both modalities measure different neural activities with different speeds. EEG provides in real time a direct measure of the changes in electrical potential occurring in the brain, while fMRI indirectly estimate brain activity by measuring changes in BOLD signal reflecting neurovascular activity, which occurs in general few seconds after a neural event [7]. Few studies have investigated, and found some correlations between EEG signal and BOLD activity, in specific and simple tasks. Some early studies reported negative correlation between the BOLD signal in the occipital lobe and the alpha rhythm (7-13Hz) in occipital electrodes during eyes open - eyes closed tasks [17,8], showing first potential link between EEG and fMRI, yet in some specific locations during specific simple tasks.

In the literature, the term EEG-informed fMRI can be found to describe methods extracting relevant features from EEG signals in order to derive a predictor of the associated BOLD signal in the region of interest under study. A recent review [1] gives a good overview of the principal EEG-informed fMRI methods and their limitations. Different strategies have been investigated, depending on the type of activity under study (epilepsy, resting state, open/closed eyes, relaxation): either by selecting one channel on interest, either by using multiple channels, before extracting features of interest. For example in [13,6], authors used a temporal independent component analysis to select the channel reflecting the best the epileptic seizures. In [26], authors used a spatial, spectral and temporal decomposition of the EEG signals to map EEG on BOLD signal changes in the thalamus. From a more symmetrical way, we proposed in [19], a method for the estimation of brain source activation, improving its spatio-temporal resolution, compared to EEG or BOLD fMRI only.

However, in the context of neurofeedback, using simultaneous recording of EEG-fMRI to estimate neurofeedback scores computed from features of both modalities (NF-EEG-fMRI) is a recent application that have been first introduced, and its feasibility demonstrated by [31,22,15]. The methodology to synchronise both signals for real time neurofeedback is new [15], allowing the acquisition of new NF-EEG-fMRI data, such as the one we will be using for this study [22]. To export NF-fMRI scores outside the scanner, most of the methods intend to predict the fMRI BOLD signal activity on a specific region of interest by learning from EEG signal recorded simultaneous, inside the fMRI scanner. For example the method proposed in [16], uses a ridge regression model with a ℓ_2 regularisation, based on a time/frequency/delay representation of the EEG signal from a single channel. Results show a good estimation of the BOLD signal in the region of interest, but the use of the neurofeedback in this study is only to serve the paradigm, making this work part of the EEG-informed methods. The neurofeedback is not used to be learnt or improved as we are proposing here here.

Besides it has been shown in [22], that the quality of neurofeedback session is improved when using simultaneously both modalities, in NF-EEG-fMRI sessions. Being able to reproduce in real time a NF-EEG-fMRI session when using EEG only, would reduce the need of fMRI in neurofeedback, while increasing the quality of NF sessions.

Our challenge here, is to learn activation patterns (see section 2.2) from simultaneous EEG-fMRI recording, performed during hybrid NF-EEG-fMRI sessions, to improve the quality of neurofeedback scores when EEG is used alone. The motivation of this is multiple: since we are considering a new kind of data, we want to provide a simple method characterising NF-EEG-fMRI in EEG, leading to understandable model to confirm existing relations between EEG and fMRI in neurofeedback scores, or to discover new relationships. Neurofeedback features in fMRI come from the BOLD activation in one or more region of interest. We propose an original alternative to source reconstruction in the context of neurofeedback. Indeed we directly intent to predict NF scores, without dealing with source reconstruction or spatial filtering to estimate BOLD-fMRI signal first on a specific region of interest, as proposed in a previous method [19]. To our knowledge, this problem of prediction of hybrid neurofeedback scores (without source reconstruction) is new, and has not been explored yet in the literature. Also we want the activation pattern to be applicable in real-time when using new EEG data. The main objective of this paper is to design a method able to exploit EEG only, and predict an NF score of quality comparable to the NF score that could be achieved with a combination of EEG and fMRI. The approach is based on a machine learning mechanism. During a training phase, both EEG and fMRI are simultaneously acquired and used to compute and synchronise, in real time, NF-EEG and NF-fMRI scores, both being combined into an hybrid NF-EEG-fMRI score. EEG signals and NF scores are used to learn activation patterns. During the testing phase, the learned activation pattern is applied to unseen EEG data, providing simulated NF-EEG-fMRI scores in real time. Sparse re-

gression is exploited to build a NF-predictor. The NF-predictor is composed by a model and a design matrix, it takes as inputs EEG signals with a reference NF scores and a test EEG signal. It provides as outputs a prediction of NF scores on the test EEG signal. The design matrix is composed by EEG features estimated from different frequency bands with different delay on each EEG channel. The model uses an adapted prior for brain activation patterns, using a mixed norm giving a structured sparsity, to spatially select electrodes and then select the corresponding frequency bands.

In section 2 we present the proposed model and the methods used to solve it. Then we will experiment our learning model on neurofeedback sessions with motor imagery task, which unique data are presented in section 3. Section 4 presents results on a group of 17 subjects with 3 NF sessions of motor imagery each, and compared the results to a widespread learning method, used in Brain Computing Interface to discriminate two mental states, the Common spatial pattern (CSP). Section 5 provides a discussion of the proposed framework.

2 Problem and method

The approach consists in considering that, during a training phase, we have access to reference scores $y(t)$ and a temporal representation (potentially non-linear) of EEG signals $\boldsymbol{X}$ (called a design matrix, presented in section 2.1), and wish to choose a parameter vector $\boldsymbol{\alpha}$ such that $y(t) \approx q(\boldsymbol{X}(t), \boldsymbol{\alpha})$ for all t, where q is some parametric function. $\boldsymbol{\alpha}$ is a matrix matching the size of $\boldsymbol{X}(t)$, here we consider

$$q(\boldsymbol{X}(t), \boldsymbol{\alpha}) := \langle \boldsymbol{X}(t), \boldsymbol{\alpha} \rangle = \sum_{i=1}^{E} \sum_{j=1}^{F} \boldsymbol{X}_{i,j}(t) \boldsymbol{\alpha}_{i,j}.$$

Regularisation is used to select an optimal parameter vector $\widehat{\boldsymbol{\alpha}}$ that fits the training data, while avoiding over-fitting, as detailed in Section 2.2.

Only a few brain regions are expected to be activated by a given cognitive task, therefore the electrodes configuration is said to be spatially sparse. However frequency bands of each electrodes are not necessarily sparse, and might even be smooth depending on the frequency band sampling.

From here, we will use the following notations. $y_{\mathrm{e}}(t) \in \mathbb{R}, \forall t \in \{1, ..., T\}$ are the T neurofeedback scores estimated from EEG signals (noted $S_{\mathrm{EEG}} \in \mathbb{R}^{E \times T_{\mathrm{EEG}}}$), measured from E electrodes during T_{EEG} samples of time. $y_{\mathrm{f}}(t) \in \mathbb{R}, \forall t \in \{1, ..., T\}$ are the T neurofeedback scores extracted from Blood Oxygen Level Dependent imaging (BOLD) signal of functional-MRI acquisitions $S_{\mathrm{fMRI}} \in \mathbb{R}^{V \times T_{\mathrm{fMRI}}}$, with V the number of voxels and T_{fMRI} the number of acquired volumes. $y(t) \in \mathbb{R}, \forall t \in \{1, ..., T\}$ is a set of neurofeedback scores that can be y_{e}, y_{f} or $y_{\mathrm{c}} = y_{\mathrm{e}} + y_{\mathrm{f}}$ a combination of both (more details are provided in section 3). First, relevant information from EEG data need to be extracted and organised to form what we call a design matrix.

2.1 Structured design matrices from EEG signal

The design matrix $\boldsymbol{X}_0 \in \mathbb{R}^{T\times E\times B}$, where E is the number of electrodes and B the number of frequency bands, contains relevant information extracted from the EEG signal. Each temporal matrix of $\boldsymbol{X}_0$, $\boldsymbol{X}_0(t) \in \mathbb{R}^{E\times B}\, \forall t \in \{1;\ldots;T\}$ is a frequency decomposition corresponding to the past 2 seconds of S_{EEG}. We used a Hamming time window of 2 seconds, to estimate the average *power* of each frequency band $b \in \{1;\ldots;B\}$ (defined below) on each channel $\in \{1;\ldots;E\}$. Each time window of EEG signal is overlapped by 1.75 seconds (0.25 seconds shift), to match with the 4Hz sample of the $\boldsymbol{y}$ values. The B frequency bands have an overlap of 1 Hz with the next band, and are defined between a minimum frequency b_{min} Hz and a maximum frequency b_{max} Hz (see section 3). We chose to use several relatively narrow frequency bands to let the model select the relevant bands for each electrodes. Furthermore it has been suggested [18,25] to use different frequency bands when working with coupling EEG-fMRI data.

The model also has to be able to predict y_{f} scores, derived from BOLD signal (see section 3). There is no linear relationship between BOLD signal and average power on frequency bands from EEG signal. Therefore, to better match y_{f} scores, we decided to apply a non-linear function to $\boldsymbol{X}_0$, used in fMRI to model BOLD signals [21,14], the canonical Hemodynamic Response function (HRF). We convolved $\boldsymbol{X}_0$ on its temporal dimension with the HRF, formed by 2 gamma functions, for a given delay of the first gamma function to compensate the response time of BOLD signal, as suggested in [16]. The HRF will temporally smooth and give a BOLD-like shape to the design matrix and increase a potential linear relationship between y_{f} and design matrix. Since HRF is known to vary considerably across brain regions and subjects [12], it is therefore recommended to consider different delays, but also to chose a range of values corresponding to the task asked. For the type of task addressed in the experimental part, the observed delay is around 4 seconds, therefore we convolved $\boldsymbol{X}_0$ with 3 differents HRF leading to 3 new design matrices $\boldsymbol{X}_3, \boldsymbol{X}_4, \boldsymbol{X}_5$ with respectively a delay of 3, 4 and 5 seconds for the canonical HRF.

Those design matrices are concatenated in their 2nd dimension to form the $\boldsymbol{X}_c \in \mathbb{R}^{T\times M\times B}$ matrix, with $M = 4 * E$. Therefore, for each time t, $\boldsymbol{X}_c(t) = [\boldsymbol{X}_0(t); \boldsymbol{X}_3(t); \boldsymbol{X}_4(t); \boldsymbol{X}_5(t)]$. We also denote $\boldsymbol{X}_d(t) = [\boldsymbol{X}_3(t); \boldsymbol{X}_4(t); \boldsymbol{X}_5(t)]$ the design matrix of the different delays.

2.2 Optimisation

EEG data are now represented into a structured design matrix $\boldsymbol{X}_c$, we can search for a weight matrix $\hat{\boldsymbol{\alpha}} \in \mathbb{R}^{M\times B}$, such that $\sum_{m,h} \hat{\boldsymbol{\alpha}}(m,h)\boldsymbol{X}_c(t,m,h)$ estimates as well as possible the NF score $y(t), \forall t \in \{1;\ldots;T\}$. Note: the methodology is presented for the design matrix $\boldsymbol{X}_c$, but can be used for $\boldsymbol{X}_0$ or $\boldsymbol{X}_d$.

To identify the $\hat{\boldsymbol{\alpha}}$, called activation pattern, we propose the following strategy, which consists in learning, for a given subject and a NF session, the optimal $\hat{\boldsymbol{\alpha}}$

by solving the following problem:

$$\widehat{\boldsymbol{\alpha}} = \underset{\boldsymbol{\alpha}}{\operatorname{argmin}} \sum_{t=1}^{T} \frac{1}{2}\big(y(t) - q(\boldsymbol{X}_c(t), \boldsymbol{\alpha})\big)^2 + \phi_\lambda(\boldsymbol{\alpha}) \tag{1}$$

with ϕ_λ a regularisation term, λ a weighting parameter for the regularisation term. This $\hat{\boldsymbol{\alpha}}$ is then applied to a design matrix $\boldsymbol{X}_c^{test}$ from a new session, to predict its NF scores

$$\tilde{y}_{\widehat{\boldsymbol{\alpha}}}(t) = q({\boldsymbol{X}_{\boldsymbol{c}}}^{test}(t), \widehat{\boldsymbol{\alpha}}) \ \forall t \in \{1; \ldots; T\}.$$

Equation (1) is of the form $\operatorname{argmin}(g_1(\boldsymbol{\alpha}) + g_2(\boldsymbol{\alpha}))$ and its resolution can be done using the Fast Iterative Shrinkage Thresholding Algorithm (FISTA) [3], which is a two-step approach of the Forward-Backward algorithm [5] making it faster. FISTA requires the same conditions as the Forward-Backward algorithm, meaning a convex differentiable with Lipschitz gradient term g_1 and a convex term g_2 that is not necessarily differentiable but smooth enough to make its proximal map computable.

Here $g_1(\boldsymbol{\alpha}) = \sum_t^T \frac{1}{2}(y(t) - q(\boldsymbol{X}_c(t), \boldsymbol{\alpha}))^2$ is a sum of convex and differentiable functions with

$$\bigtriangledown g_1(\boldsymbol{\alpha}) = \sum_t -\boldsymbol{X}_c(t)(y(t) - q(\boldsymbol{X}_c(t), \boldsymbol{\alpha}))$$

since $\forall i \in \{1; \ldots; M\}, j \in \{1; \ldots; B\}, [\frac{\partial q(\boldsymbol{X}_c(t), \boldsymbol{\alpha})}{\partial \boldsymbol{\alpha}(i,j)}]_{i,j} = \boldsymbol{X}_c(t, i, j)$. By representing $\boldsymbol{X}_c(t)$ and $\boldsymbol{\alpha}$ as vectors of size $M * B$, we can easily note that $\frac{\partial g_1}{\partial \boldsymbol{\alpha}}$ is a sum of Lipschitz functions. Therefore, the Lipschitz constant of $\frac{\partial g_1}{\partial \boldsymbol{\alpha}}$ is $L = \|X_V^\intercal X_V\|$ with $X_V \in \mathbb{R}^{T*M*B}$ the vectorised version of $\boldsymbol{X}_c$.

The NF-predictor uses structured design matrix to have a better control on the interpretation of results and to better optimise the weights $\hat{\boldsymbol{\alpha}}$. Therefore we have to adopt an optimisation strategy coherent with this structure. The activation pattern of the NF-predictor:

1. has to be spatially sparse since the cognitive task is reflected by brain activity from a limited set of electrodes,
2. has to be smooth across different overlapped frequency bands,
3. has to allow non-relevant frequency bands to be null.

The term g_2 is the prior term. Here, for $g_2(\boldsymbol{\alpha}) = \phi_\lambda(\boldsymbol{\alpha})$, we chose to use a ℓ_{21} mixed norm [20] followed by a ℓ_1-norm (noted ℓ_{21+1}-norm in [10]) to fit all structure conditions mentioned above.

$$\phi_\lambda(\boldsymbol{\alpha}) = \lambda\|\boldsymbol{\alpha}\|_{21} + \rho\|\boldsymbol{\alpha}\|_1$$

with $\rho \in \mathbb{R}^+$ and $\lambda \in \mathbb{R}^+$. We chose not to estimate the parameter ρ, to keep computation time reasonable. Indeed, ρ weights the induced spatial sparsity over EEG channels, and we chose to fix this parameter for all subjects, as we

hypothesis that there is no reason, for the number of electrodes involved in the activation pattern, to significantly change between subjects. However the estimation of λ parameter is needed (since we do not have hypothesis on its behaviour) and presented in the next section. The ℓ_{21} mixed norm that writes $\|\boldsymbol{\alpha}\|_{21} = \sum_m \sqrt{\sum_b \alpha_{m,b}^2}$ satisfies conditions 1) and 2). The ℓ_1 norm defined as $\|\boldsymbol{\alpha}\|_1 = \sum_{m,b} |\alpha_{m,b}|$ satisfies condition 3) since ℓ_p norms with $p \leq 1$ are known to promote sparsity. The last key point of FISTA algorithm is the proximal map associated to the ℓ_{21+1} norm $\text{Prox}_{\ell_{21+1}} : \mathbb{R}^{M\times B} \to \mathbb{R}^{M\times B}, \boldsymbol{\beta} \mapsto \text{argmin}_{\boldsymbol{\alpha}}(\phi_\lambda(\boldsymbol{\alpha}) + 1/2\|\boldsymbol{\beta} - \boldsymbol{\alpha}\|^2)$, defined as

$$(\text{Prox}_{\ell_{21+1}}(Y))_{m,b} = \frac{Y_{m,b}}{|Y_{m,b}|}(|Y_{m,b}| - \rho)^+(1 - \frac{\lambda}{\sqrt{\sum_b(|Y_{m,b}| - \rho)^{+2}}})^+$$

with operator $(.)^+ = max(., 0)$. One can note that by cancelling either the λ parameter or the ρ parameter, we retrieve the proximal map associated to the ℓ_{21} (when $\rho = 0$) and to the ℓ_1 norm (when $\lambda = 0$), which demonstrations can be found in the appendix of [9]. For the stopping criterion of FISTA, a large enough number of iteration has been used, allowing the model to converge before reaching the last iteration. All elements and conditions are gathered to run the FISTA algorithm.

2.3 $\boldsymbol{\lambda}$ parameter selection

The parameter λ is important in the optimisation problem and we decided to estimate it automatically. The following process chooses the best λ among a list of $\Lambda = \{\lambda_1; ...; \lambda_l\}$ sorted in increasing order. First of all, the data must be split into 2 sets, a learning set and a testing set. For each value λ_i of Λ, the learning set, formed by L neurofeedback scores with their associated design matrices, is divided $K = 50$ times into a training set of size $R_k = 90\%L$ and a cross-validation set of size $CV_k = 10\%L$ composed by the remaining 10% of the learning set. A model $\hat{\boldsymbol{\alpha}}^{(k,i)}$ is estimated on the training dataset k composed by R_k neurofeedback scores $y(j)$ and the associated design matrices $\boldsymbol{X}_c(j)$ with λ_i, i.e.:

$$\hat{\boldsymbol{\alpha}}^{(k,i)} = \arg\min \sum_j \| y(j) - q(\boldsymbol{X}_c(j), \hat{\boldsymbol{\alpha}}^{(k,i)})\|^2 + \lambda_i \|\boldsymbol{\alpha}^{(k,i)}\|_{21} + \rho\|\boldsymbol{\alpha}^{(k,i)}\|_1$$

with $j \in R_k$ and $\boldsymbol{X}_c(j) \in \mathbb{R}^{M\times B}$. For the current λ_i evaluation, we stop the process when $\sum_k |\hat{\boldsymbol{\alpha}}^{(k,i)}|_0/K < 2$. There is no need to investigate the next λ_i, the current one is sparse enough, and the next one might lead to null models.

We then apply the model $\hat{\boldsymbol{\alpha}}^{(k,i)}$ to the corresponding cross-validation set of CV_k NF scores, to obtain estimated values of $y(s)$, $\tilde{y}(s) = q(\boldsymbol{X}_c(s), \hat{\boldsymbol{\alpha}}^{(k,i)})$, with $s \in CV_k$. For each one of the 50 partitioning into training and cross-validation sets, we computed the normalised mean squared error NMSE for a given set of data $\{y, \boldsymbol{X}_c\}$, for the training sets and the cross-validation sets.

$$\text{NMSE}(\{y, \boldsymbol{X}_c\}, \hat{\boldsymbol{\alpha}}^{(k,i)}) = \frac{\sum_s (y(s) - q(\boldsymbol{X}_c(s), \hat{\boldsymbol{\alpha}}^{(k,i)}))^2}{\sum_s (y(s) - \overline{y})^2} \tag{2}$$

with $\bar{y} = 1/n \sum_s^n y(s)$. The optimal $\hat{\lambda}$ parameter is defined as the one minimising the error during training and validation. Considering only the errors from the training set $\mathrm{NMSE}(\{y(R_k), \boldsymbol{X}_c(R_k)\}, \hat{\boldsymbol{\alpha}}^{(k,i)})$ would introduce bias, and considering only the error of the cross-validation set $\mathrm{NMSE}(\{y(CV_k), \boldsymbol{X}_c(CV_k)\}, \hat{\boldsymbol{\alpha}}^{(k,i)})$, would introduce variance. Then the optimal $\hat{\lambda}$ is the λ_i that minimises :

$$\sum_{k=1}^{K} [\mathrm{NMSE}(\{y(R_k), \boldsymbol{X}_c(R_k)\}, \hat{\boldsymbol{\alpha}}^{(k,i)}) + \mathrm{NMSE}(\{y(CV_k), \boldsymbol{X}_c(CV_k)\}, \hat{\boldsymbol{\alpha}}^{(k,i)})]$$

$\hat{\lambda}$ parameter is the optimal parameter used for the model estimation. If there are several candidates, to favor sparsity, the larger of these candidate is chosen.

3 Data acquisition and pre-processing

We used a group of 17 subjects that were scanned using a hybrid Neurofeedback platform coupling EEG and fMRI signal [15]. A 64-channel MR-compatible EEG solution from Brain Products (Brain Products GmbH, Gilching, Germany) has been used, the signal was sampled at 5kHz, FCz is the reference electrode and AFz the ground electrode. For the fMRI scanner, we used a 3T Verio Siemens scanner with a 12 channels head coil (repetition time (TR) / echo time (TE) = 2000/23ms, FOV = $210 \times 210\mathrm{mm}^2$, voxel size = $2 \times 2 \times 4\mathrm{mm}^3$, matrix size $=105 \times 105$ with 16 slices, flip angle = 90°). All subjects are healthy volunteers, right-handed and had never done any neurofeedback experiment before. They all gave written informed consent in accordance with the Declaration of Helsinki as specified in the study presenting the data used here [22]. They all had 3 NF motor imagery sessions of 320 seconds each, after a session dedicated to the calibration. One session consists in 8 blocks alternating between 20 seconds of rest, eyes open, and 20 seconds of motor imagery of their right hand. The neurofeedback display was uni-dimensional (1D) for 9 subjects (Figure 1 left), and bi-dimensional (2D) for 8 subjects (Figure 1 middle). For both, the goal was to bring the ball into the dark blue area [23].

NF scores y_e and y_f being from different modalities, were standardised before summing to form y_c. In this study NF scores refer to standardised scores, except when they are predicted. For this study, y_e have been computed from the commonly used, in neurofeedback, the Laplacian operator, centred around the region of interest, channel C3 here. For each time interval I_t the spatial filtering is noted Lap(C3, I_t). The temporal segments I_t are spaced by 250ms, and a length of 2 seconds (therefore an overlapping of 1,75 seconds), as for the design matrix construction. The power of the frequency band [8Hz - 30Hz] is then extracted via the function f:

$$y_\mathrm{e}(t) = -f_{[8-30]}(\mathrm{Lap}(\mathrm{C3}, I_t))$$

One may note the presence of the minus operator, used here for the sake of coherence with y_f (Figure 1 right).

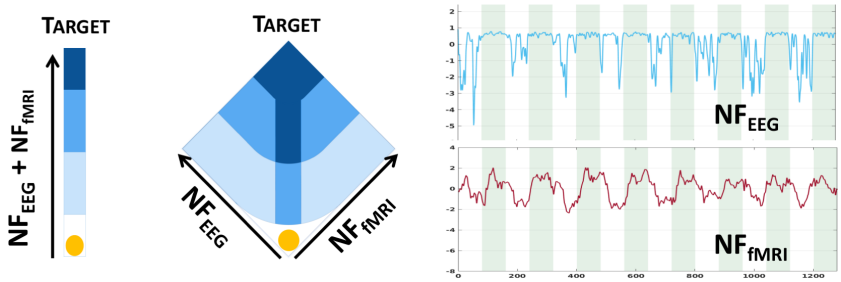

Fig. 1. Bi-modal neurofeedback strategies (1D on the left, 2D on the middle), displayed during sessions [23]. 1D: the ball's position represents the average score between y_{e} and y_{f}. 2D: the left axis represents the y_{e} and the right axis represents the y_{f} scores. The 2 plots on the right show NF scores from EEG and from fMRI, green areas are task, white areas are rest. The goal is to bring the ball in the dark blue area.

The neurofeedback scores y_{f} have been computed from the maximal intensity of BOLD signal covering the right-hand motor area and the supplementary motor area, one score is computed per volume acquired (i.e 1 per second). Then scores y_{f} are re-sampled and smoothed (using a Savitzky-Golay filter, known to avoid signal distortion) to fit the 4Hz y_{e} scores ($T = 1280$).

Here we introduce an other neurofeedback score, $\hat{y}_{\mathrm{CSP}}(t) \in \mathbb{R}, \forall t \in \{1, ..., T\}$, to be compared to our method, scores estimated from the Common Spatial Pattern (CSP) algorithm known to be efficient despite its sensitivity to noise [24]. The CSP is a widely used filter in braincomputer interface to discriminate two mental states using EEG signals, and sometime used in the context of neurofeedback [15,22]. Here, EEG signal are being recorded simultaneously with fMRI, the two mental states are the 20 seconds resting blocks and the 20 seconds task blocks, modulated by the neurofeedback scores y_{e} and y_{f} received by the subject. The CSP filter is used to spatially filter the EEG signal, as for the Laplacian and with the same time intervals I_t, the power of the frequency band 8-30 Hz is estimated on the filtered signal to obtain the $\hat{y}_{\mathrm{CSP}}$ values.

An active set have been selected on design matrices to avoid potentially correlated noise, due to head movement during resting blocks, obstructing signal from channels of interest. Indeed in coupling EEG-fMRI acquisitions, subjects are lying into the MRI scanner, therefore outer electrodes can be in contact with the bed or holds. We excluded outer electrodes and kept 28 electrodes, the 3 central lines have 7 electrodes (FCz is the reference), 3 frontal electrodes and 3 posterior electrodes.

For frequency bands of the design matrix $\boldsymbol{X}_0$ construction (cf section 2) and therefore for the other design matrices, we chose $b_{min} = 8$, $b_{max} = 30$ to cover alpha and beta frequency bands involved in motor tasks. There is $B = 10$ frequency bands, leading to bands of 3 Hz wide (with an overlap of 1Hz).

4 Experiments and Results

As said in the previous section, we have 3 neurofeedback sessions per subjects. For each subjects, we will consider 1 session as learning set, and the 2 others as testing sets. Leading to 3 different learning sets, and 6 different testing sets per subjects. Potential outliers in the design matrices (i.e. observations > mean±3std) were thresholded in the learning set, and bad observations from annotations on the EEG signal were removed as their corresponding NF scores.

4.1 Experiments and validation

We tested different NF-predictors (input: an EEG signal, a reference NF scores and a testing EEG signal, and output: the predicted NF scores for the testing EEG signal) for the prediction of different NF scores, $\forall t \in \{1; \ldots; T\}$:

- NF-predictor 1: $\tilde{y}_{\widehat{\boldsymbol{\alpha}}_{\mathrm{c}}}(t) = q(\boldsymbol{X}_c^{test}(t), \hat{\boldsymbol{\alpha}}_c)$ with $\hat{\boldsymbol{\alpha}}_c$ (eq. 1), learned from $\boldsymbol{X}_c$ and y_{c}
- NF-predictor 2: $\tilde{y}_{\widehat{\boldsymbol{\alpha}}_{\mathrm{e}}}(t) = q(\boldsymbol{X}_0^{test}(t), \hat{\boldsymbol{\alpha}}_e)$ with $\hat{\boldsymbol{\alpha}}_e$ (eq. 1), learned from $\boldsymbol{X}_0$ and y_{e}
- NF-predictor 3: $\tilde{y}_{\widehat{\boldsymbol{\alpha}}_{\mathrm{f}}}(t) = q(\boldsymbol{X}_d^{test}(t), \hat{\boldsymbol{\alpha}}_f)$ with $\boldsymbol{X}_d = [\boldsymbol{X}_3; \boldsymbol{X}_4; \boldsymbol{X}_5]$, and $\hat{\boldsymbol{\alpha}}_f$ (eq. 1), learned from $\boldsymbol{X}_d$ and y_{f}
- NF-predictor 4 :$\tilde{y}_{\widehat{\boldsymbol{\alpha}}_{\mathrm{e}}}(t) + \tilde{y}_{\widehat{\boldsymbol{\alpha}}_{\mathrm{f}}}(t)$ using NF-predictor 2 and NF-predictor 3
- NF-predictor 5: $y_{\mathrm{e}}(t) + \tilde{y}_{\widehat{\boldsymbol{\alpha}}_{\mathrm{f}}}(t)$ using NF-predictor 3 only

The NF-predictors 4 and 5 permit the use of the 2D score visualisation (Figure 1) to display NF scores. NF-predictor 4 is to compare to NF-predictor 1, since one directly learn the y_{c}, and the other cut the problem into 2 problems, NF predictors 2 and 3. NF-predictor 5 is an other alternative, in which only the NF-fMRI scores are learned from EEG signal. We run the following experiments to test our different NF-predictors:

- Model validation: we used the learning set to assess if the NF-predictors could model accurately the NF scores. For each subject and each NF-predictor, we estimated correlations with the reference NF score to quantify the quality of prediction. For the validation, we compared to the correlation of y_{e} to y_{c} which is part of the y_{c} score, to have a correlation reference, and to know if, in the validation process, the model can do better than y_{e}.
- Model prediction: we apply the learned activation patterns to a new testing set. For each subject and each pair of session (6 learning/testing pair per subject), we compared correlations between each NF-predictor. We also compared the different predictions to the prediction given by the widely used, in brain computing interface, CSP filter [24], introduced in section 3.
- To observe the captured structure in the activation pattern $\hat{\boldsymbol{\alpha}}_c$ learned with NF-predictor 1, we split the averaged, over subjects and sessions, activation pattern into matrices corresponding to the design matrices composing $\boldsymbol{X}_c$, and displayed results of the first dimension (electrodes) and of the second dimension (frequency bands).

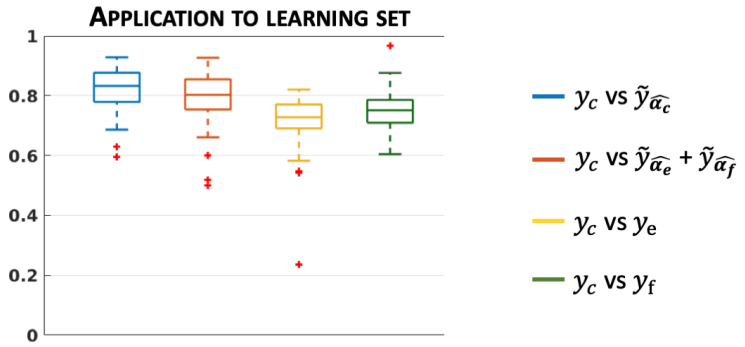

Fig. 2. Model validation compared to the NF scores (y_e and y_f), as reference. Boxplots (median and quartiles) of Pearson's correlation coefficients over all subjects and sessions, between NF-predictors and y_c.

4.2 Results

The validation of the NF-predictors (i.e. the learned activation patterns $\hat{\boldsymbol{\alpha}}$ are applied to the learning set) results are shown at Figure 2. Pearson's correlation coefficients between the prediction and the ground truth are computed for each of the 3 learning sessions and for all subjects. The estimated $\tilde{y}_{\widehat{\boldsymbol{\alpha}}_c}$ (in dark blue, median r = 0.83, mean r = 0.82), on the learning set, show stronger correlation with y_c than the reference scores y_e (mean r = 0.71. paired t-test, p$\leq$ 1e-3) y_f (mean r = 0.75. paired t-test, p$\leq$ 1e-3) and $\tilde{y}_{\widehat{\boldsymbol{\alpha}}_e}(t) + \tilde{y}_{\widehat{\boldsymbol{\alpha}}_f}(t)$ (in yellow, median r = 0.8, mean r = 0.79. paired t-test, p$\leq$ 1e-3). Furthermore, correlations are very high ($\geq$ 0.8) for $\tilde{y}_{\widehat{\boldsymbol{\alpha}}_c}$ and $\tilde{y}_{\widehat{\boldsymbol{\alpha}}_e} + \tilde{y}_{\widehat{\boldsymbol{\alpha}}_f}$, letting think that the model is adapted to the NF prediction problem. In addition, the model could fit NF-fMRI scores using only EEG signals information (median r = 0.80 for $\tilde{y}_{\widehat{\boldsymbol{\alpha}}_f}$ vs y_f). This is promising for the proposed NF-predictor 5 which only requires the prediction of NF-fMRI scores and EEG signals only.

During the testing phase (Figure 3), the learned activation patterns are applied to the testing sets, i.e. the 2 other unseen NF sessions for each one of the 3 NF sessions. During the learning session, if a subject focused more on NF-fMRI (which is the easiest one to control) than on NF-EEG, the EEG-signals might lose coherence with respect to the NF-fMRI scores. Even though, the EEG signals could predict NF-fMRI scores with a correlation of 0.32 in median and mean 0.3, which is a fair correlation between such different modalities. Examples of NF prediction are given at Figure 5, the bottom plot shows the prediction $\tilde{y}_{\widehat{\boldsymbol{\alpha}}_f}$ of y_f on a testing set.

The purple box plot at figure 3, shows that NF-predictor 5 (median correlation = 0.74) is the best at predicting y_c, its prediction is better than y_e only (mean correlation $y_e + \tilde{y}_{\widehat{\boldsymbol{\alpha}}_f}$ vs y_c = 0.70, mean correlation y_e vs y_c = 0.67). A one sided paired t-test (which alternative hypothesis is y_e has a lower correlation to y_c than $y_e + \tilde{y}_{\widehat{\boldsymbol{\alpha}}_f}$), gives a p-value $p = 0.01$, meaning that the prediction $\tilde{y}_{\widehat{\boldsymbol{\alpha}}_f}$

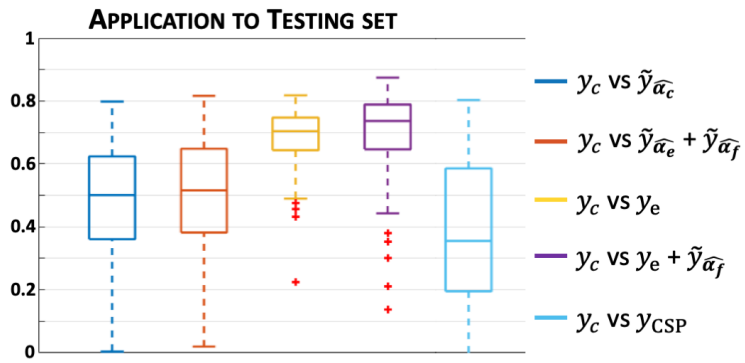

Fig. 3. Model testing; For each subject, application of learned pattern to an unknown session. Boxplots (median and quartiles) of Pearson's correlation coefficients over all subjects and sessions, between NF-predictors and y_c. The comparison of y_e vs $y_c = y_e + y_f$ (yellow, middle) is here only as a reference, since y_e is on both sides. The light blue box (right) shows correlation of y_c with the learned CSP filter (see section 3).

significantly adds information to y_e. An example of $y_e + \tilde{y}_{\widehat{\alpha}_f}$ vs y_c is given at Figure 4, right top.

Figure 3 also shows (in light blue on right side) that the predicted $\hat{y}_{CSP}$ have a lower correlation with the reference scores y_c. The correlation $\hat{y}_{CSP}$ vs y_c is significantly lower than the correlation of any of the proposed NF-predictor with y_c. One sided paired t-tests (alternative hypothesis being $\hat{y}_{CSP}$ has a lower correlation to y_c than the considered NF-predictor) give the following p-values: for NF-predictor 1 (dark blue box on Figure 3) we found a value $p =$ 3e-6, for NF-predictor 4 (red box on Figure 3) $p =$ 2e-7, and for NF-predictor 5 (purple box on Figure 3) $p =$ 1e-27. The fact that the CSP, which discriminates 2 mental states, cannot correctly predict the scores of a subject on a test session, confirms that considered signals are too noisy here. Subjects can sometimes be more receptive to the EEG and sometimes to the BOLD signal, and those changes are only captured by the different neurofeedback scores obtained during the learning phase.

Figure 4 shows that, even if the correlations of $\tilde{y}_{\widehat{\alpha}_c}$ (and $\tilde{y}_{\widehat{\alpha}_e} + \tilde{y}_{\widehat{\alpha}_f}$ too) are lower than $y_e + \tilde{y}_{\widehat{\alpha}_f}$ (cf box plots at Figure 3), $\tilde{y}_{\widehat{\alpha}_c}$ can predict correctly the reference score y_c. We do not show the prediction of $\tilde{y}_{\widehat{\alpha}_e} + \tilde{y}_{\widehat{\alpha}_f}$, but it has the same aspect as $\tilde{y}_{\widehat{\alpha}_c}$ on Figure 4. The correlations (of NF-predictors 1 and 4) are lower than y_e, because y_e is part of the reference score (as is y_e in $y_e + \tilde{y}_{\widehat{\alpha}_f}$), and also the regularisation of the model is smoothing the prediction of the NF-predictors. The box plot for y_e vs $y_c (= y_e + y_f)$ (yellow, Figure 3) is only here to have a point of comparison when learning phase is not done and the fMRI is not considered. The high correlation of y_e with y_c illustrates the high frequency changes of y_e scores, which are not necessarily information. However, it can be observed that interestingly, both NF-predictors (1 and 4) equally predict y_c. This

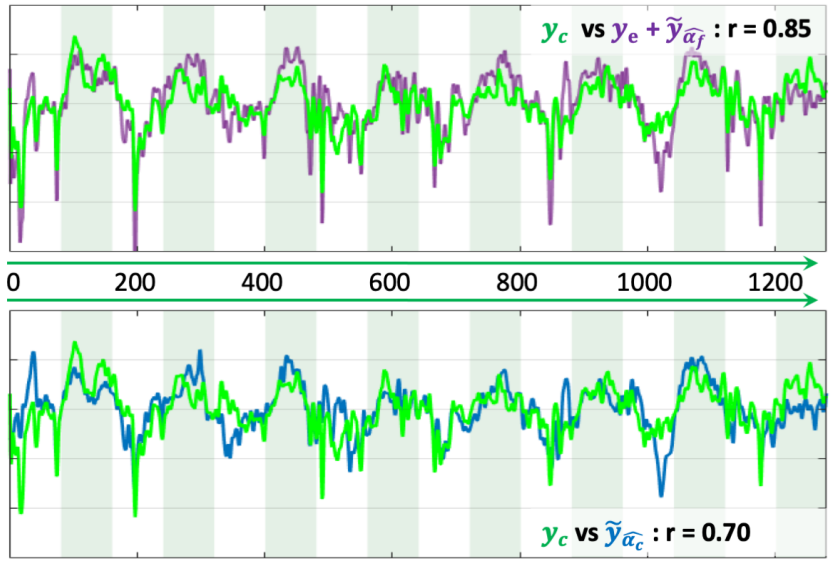

Fig. 4. Examples of prediction of NF scores. Vertical bands indicate the rest and the task blocks. The correlation coefficient r indicates the correlation between each pair of time-series NF scores. The ground truth (y_c) is in green, the x-axis is the temporal axis in milliseconds. Top: NF-predictor 5 in purple. Bottom: NF-predictor 1 in blue.

might not be expected since λ parameters are estimated independently for each model.

To observe the distribution, over sessions and subjects, of the learned nonzeros coefficients, we first denote $\hat{\boldsymbol{\zeta}}_c = \sum_j^{17} \sum_{s_1,s_2}^{3} |\hat{\boldsymbol{\alpha}}_c^{(j,s_1,s_2)}| \in \mathbb{R}^{M\times B}$ the absolute activation pattern, and $\hat{\gamma}_c = \sum_j \sum_{s_1,s_2}^{3} \hat{\boldsymbol{\alpha}}_c^{(j,s_1,s_2)} \in \mathbb{R}^{M\times B}$ the average activation pattern. By construction of the design matrix $\boldsymbol{X}_c$, $\hat{\boldsymbol{\alpha}}_c$ can be split into 4 activation patterns, and therefore, we can display heat maps for the 4 absolute activation patterns $\in \{1;\ldots;E\}$ (Figure 6, top line) $\sum_{b\in B} \widehat{\boldsymbol{\zeta}}_0, \sum_b \widehat{\boldsymbol{\zeta}}_3, \sum_b \widehat{\boldsymbol{\zeta}}_4$ and $\sum_b \widehat{\boldsymbol{\zeta}}_5$; and color maps of the 4 average patterns $\sum_b \widehat{\boldsymbol{\gamma}}_0, \sum_b \widehat{\boldsymbol{\gamma}}_3, \sum_b \widehat{\boldsymbol{\gamma}}_4$ and $\sum_b \widehat{\boldsymbol{\gamma}}_5$ showing the sign of the strongest and stable coefficients across subjects and sessions. Interestingly, the most intense heat map, $\sum_b \widehat{\boldsymbol{\zeta}}_0$ with a maximum value of 45, concentrates its non-zero values on C3 channel (above the right-hand motor area) and corresponds to the design matrix $\boldsymbol{X}_0$, directly extracted from EEG signal without temporal delay. The next heat map in intensity order is $\sum_b \widehat{\boldsymbol{\zeta}}_5$ with two peaks above the visual cortex (Pz and P4 channels). All maps are sparse and present different distributions of the non-zero values. It is also interesting to observe that the main activation peaks (C3, Pz and P4) have opposite signs, suggesting a negative correlation with a delay of 5 seconds between C3 and the posterior Pz, P4. This is not an absurd finding since NF scores are visual, subjects are focused on the visualisation of NF scores during task, and

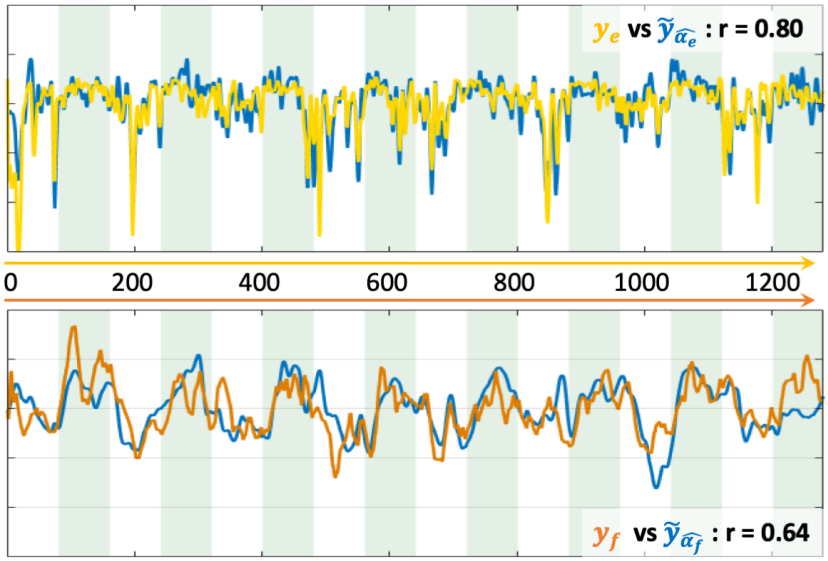

Fig. 5. Examples of prediction of NF scores. The x-axis is the temporal axis in milliseconds. Vertical bands indicate the rest and the task blocks. The correlation coefficient r indicates the correlation between each pair of time-series NF scores. Top: the ground truth y_{e} is in yellow and its estimate in blue. Bottom: the ground truth y_{f} is in orange and its estimate in blue.

rest during resting blocks (eyes open). This let think that posterior electrodes could be removed from the active set of the design matrix $\boldsymbol{X}_c$.

At last, it is also possible to display the frequency profile of each average activation patterns. The 4 frequency profiles are $\sum_{e\in\{1,\ldots,E\}}\widehat{\gamma}_0, \sum_e \widehat{\gamma}_3$, $\sum_e \widehat{\gamma}_4$ and $\sum_e \widehat{\gamma}_5$, $e \in \{1, ..., E\}$, summing weights over electrodes. Figure 7 shows that the most used frequency bands over all subjects and sessions are alpha band ([8-12] Hz) and lower beta band ([13-17] Hz), the last 4 frequency bands are not displayed since they only have null coefficients. We can observe the effect of ℓ_2 regularisation which allows continuity in the frequency bands, and the effect of the subsequent ℓ_1 regularisation which removed the smaller coefficients located in the high frequencies. When considering all activation patterns (Figure 7 right side), there is a change of sign between alpha and lower beta. Each activation pattern shows a different frequency profile, which, with Figure 6, demonstrates that all patterns have complementary information.

5 Discussion and conclusion

The validation step supports that the optimisation strategy is adapted to the model, as is the choice of the different design matrices. This is when applying the learned activation patterns to a new session (Figure 3), that predicting only

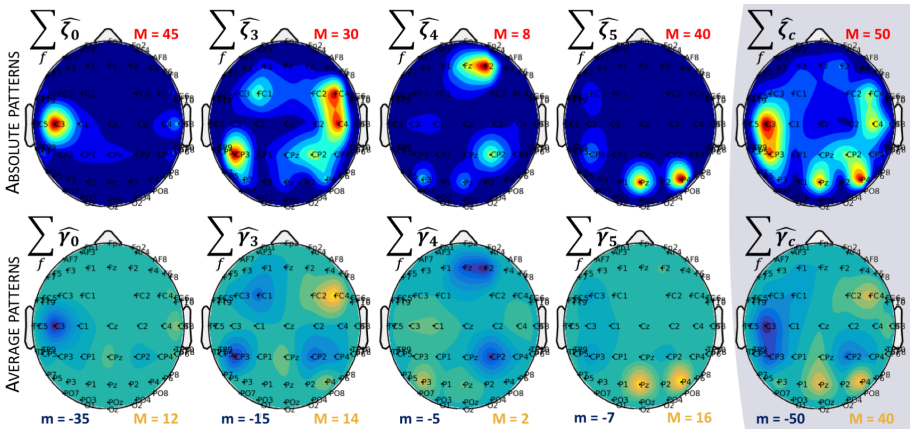

Fig. 6. Activation patterns averaged over sessions and subjects. $f \in \{1, ..., B\}$. Top line: Heat map representing the distribution of non-zero coefficients. Maximum value is indicated for each map with a red M. Bottom line: Average activation patterns, representing the sign of the main non-zero values across subject and sessions. Minimum and maximum values are indicated for each map with m and M.

NF-fMRI scores while applying a Laplacian on EEG signal appears to be the best solution. Indeed, the variability between EEG signals induces decreasing correlation for $\tilde{y}_{\widehat{\boldsymbol{\alpha}}_c}$ and for $\tilde{y}_{\widehat{\boldsymbol{\alpha}}_e} + \tilde{y}_{\widehat{\boldsymbol{\alpha}}_f}$. Predicting NF-EEG scores from EEG is not really relevant (except from a methodological point of view) since these scores are always computed from the EEG signal, which is constantly available. It is interesting to note that the 2 different strategies ($\tilde{y}_{\widehat{\boldsymbol{\alpha}}_c}$ and $\tilde{y}_{\widehat{\boldsymbol{\alpha}}_e} + \tilde{y}_{\widehat{\boldsymbol{\alpha}}_f}$) have similar results, and when decomposing the activation pattern of $\tilde{y}_{\widehat{\boldsymbol{\alpha}}_c}$, the weights corresponding to $\boldsymbol{X}_0$ are mainly located above C3, which is the centre of the Laplacian for the computation of the NF-EEG scores. Figure 6 and 7 show that only specific electrodes and frequency band (between 7 Hz and 20 Hz, higher frequencies are not captured by the model) are required, over all subjects, letting think that there is a common underlying model for the population, even if models are subject specific. To increase the prediction of NF scores, we could use more NF sessions as learning session, since as observed, EEG signals bring variability in the prediction. Each new neurofeedback session could be added to the subject-specific model.

Presently, the proposed model finds an individual model for each subject that can be seen as a personalised model for neurofeedback sessions. However, for a future work, we are investigating an adaptation of the methodology for the extraction of a common model, taking into account the differences between subjects, allowing the prediction of NF-EEG-fMRI scores on new subjects who did not participated to the model construction. This would give access to neurofeedback sessions of quality using EEG only, for subjects with MRI contraindications,

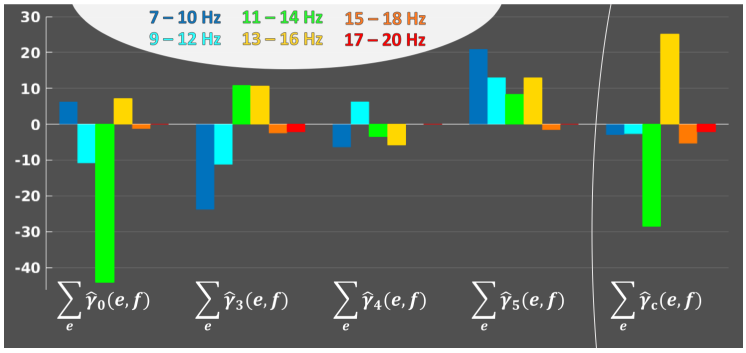

Fig. 7. Frequency profiles, across subjects and sessions, of each average activation patterns, to represent the implication of each frequency bands in the activation patterns. $e \in \{1, ..., E\}$. For each average activation pattern, the y-axis indicates the sum of weights over electrodes, for each frequency bands $f \in \{1, ..., B\}$ on the horizontal axis.

and/or drive a subject-specific model estimation, respecting the strategy used by the subject to progress in its neurofeedback task.

Other ways to improve the method proposed here would be to investigate the use of dynamic functional connectivity, a relatively recent field in BOLD fMRI which needs further investigations to be used along with EEG data [28]. Dynamic functional connectivity study the temporal fluctuations of the BOLD signal across the brain, and appears to be a promising approach in the EEG-fMRI research field [2].

To conclude, the 5th NF-predictor proposed here is able to provide prediction of the NF-fMRI scores good enough to replace the NF-fMRI scores and allows to significantly increase the quality of the estimation of NF-EEG-fMRI scores when using EEG only.

6 Acknowledgements

Data acquisition was supported by the Neurinfo MRI research facility from the University of Rennes I. Neurinfo is granted by the the European Union (FEDER), the French State, the Brittany Council, Rennes Metropole, Inria, Inserm and the University Hospital of Rennes. This work has received a French government support granted to the CominLabs excellence laboratory and managed by the National Research Agency in the Investissements d'Avenir program under reference ANR-10-LABX-07-01. It was also funded by Brittany region under HEMISFER project.

References

1. Abreu, R., Leal, A., Figueiredo, P.: EEG-Informed fMRI: A Review of Data Analysis Methods. Frontiers in Human Neuroscience **12** (Feb 2018)

2. Allen, E.A., Damaraju, E., Eichele, T., Wu, L., Calhoun, V.D.: EEG Signatures of Dynamic Functional Network Connectivity States. Brain Topography **31**(1), 101–116 (Jan 2018)
3. Beck, A., Teboulle, M.: A Fast Iterative Shrinkage-Thresholding Algorithm for Linear Inverse Problems. SIAM Journal on Imaging Sciences **2**(1), 183–202 (2009)
4. Birbaumer, N., Ramos Murguialday, A., Weber, C., Montoya, P.: Chapter 8 Neurofeedback and BrainComputer Interface. In: International Review of Neurobiology, vol. 86, pp. 107–117. Elsevier (2009)
5. Combettes, P.L., Wajs, V.R.: Signal Recovery by Proximal Forward-Backward Splitting. Multiscale Modeling & Simulation **4**(4), 1168–1200 (Jan 2005)
6. Formaggio, E., Storti, S.F., Bertoldo, A., Manganotti, P., Fiaschi, A., Toffolo, G.M.: Integrating EEG and fMRI in epilepsy. NeuroImage **54**(4), 2719–2731 (Feb 2011)
7. Friston, K.J., Jezzard, P., Turner, R.: Analysis of functional MRI time-series. Human Brain Mapping **1**(2), 153–171 (1994)
8. Goncalves, S.I., Bijma, F., Pouwels, P.W.J., Jonker, M., Kuijer, J.P.A., Heethaar, R.M., Lopes da Silva, F.H., de Munck, J.C.: A Data and Model-Driven Approach to Explore Inter-Subject Variability of Resting-State Brain Activity Using EEG-fMRI. IEEE Journal of Selected Topics in Signal Processing **2**(6), 944–953 (Dec 2008)
9. Gramfort, A., Kowalski, M., Hmlinen, M.: Mixed-norm estimates for the M/EEG inverse problem using accelerated gradient methods. Physics in Medicine and Biology **57**(7), 1937–1961 (Apr 2012)
10. Gramfort, A., Strohmeier, D., Haueisen, J., Hamalainen, M., Kowalski, M.: Functional Brain Imaging with M/EEG Using Structured Sparsity in Time-Frequency Dictionaries. In: Szkely, G., Hahn, H.K. (eds.) IPMI, vol. 6801, pp. 600–611. Springer Berlin Heidelberg, Berlin, Heidelberg (2011)
11. Hammond, D.C.: What is Neurofeedback: An Update. Journal of Neurotherapy **15**(4), 305–336 (Oct 2011)
12. Handwerker, D.A., Ollinger, J.M., D'Esposito, M.: Variation of BOLD hemodynamic responses across subjects and brain regions and their effects on statistical analyses. NeuroImage **21**(4), 1639–1651 (Apr 2004)
13. Leite, M., Leal, A., Figueiredo, P.: Transfer Function between EEG and BOLD Signals of Epileptic Activity. Frontiers in Neurology **4** (2013)
14. Lindquist, M.A., Meng Loh, J., Atlas, L.Y., Wager, T.D.: Modeling the hemodynamic response function in fMRI: Efficiency, bias and mis-modeling. NeuroImage **45**(1), S187–S198 (Mar 2009)
15. Mano, M., Lécuyer, A., Bannier, E., Perronnet, L., Noorzadeh, S., Barillot, C.: How to Build a Hybrid Neurofeedback Platform Combining EEG and fMRI. Frontiers in Neuroscience **11** (2017)
16. Meir-Hasson, Y., Kinreich, S., Podlipsky, I., Hendler, T., Intrator, N.: An EEG Finger-Print of fMRI deep regional activation. NeuroImage **102**, 128–141 (2014)
17. de Munck, J., Gonalves, S., Huijboom, L., Kuijer, J., Pouwels, P., Heethaar, R., Lopes da Silva, F.: The hemodynamic response of the alpha rhythm: An EEG/fMRI study. NeuroImage **35**(3), 1142–1151 (Apr 2007)
18. de Munck, J., Gonalves, S., Mammoliti, R., Heethaar, R., Lopes da Silva, F.: Interactions between different EEG frequency bands and their effect on alphafMRI correlations. NeuroImage **47**(1), 69–76 (Aug 2009)
19. Noorzadeh, S., Maurel, P., Oberlin, T., Gribonval, R., Barillot, C.: Multi-modal EEG and fMRI Source Estimation Using Sparse Constraints. In: Descoteaux, M., Maier-Hein, L., Franz, A., Jannin, P., Collins, D.L., Duchesne, S. (eds.) Medical

Image Computing and Computer Assisted Intervention MICCAI 2017, vol. 10433, pp. 442–450. Springer International Publishing, Cham (2017)
20. Ou, W., Hmlinen, M.S., Golland, P.: A distributed spatio-temporal EEG/MEG inverse solver. NeuroImage **44**(3), 932–946 (Feb 2009)
21. Pedregosa, F., Eickenberg, M., Thirion, B., Gramfort, A.: HRF Estimation Improves Sensitivity of fMRI Encoding and Decoding Models. In: 2013 International Workshop on Pattern Recognition in Neuroimaging. pp. 165–169. IEEE, Philadelphia, PA, USA (Jun 2013)
22. Perronnet, L., Lécuyer, A., Mano, M., Bannier, E., Lotte, F., Clerc, M., Barillot, C.: Unimodal Versus Bimodal EEG-fMRI Neurofeedback of a Motor Imagery Task. Frontiers in Human Neuroscience **11** (Apr 2017)
23. Perronnet, L., Lécuyer, A., Mano, M., Clerc, M., Lotte, F., Barillot, C.: Learning 2-in-1: towards integrated EEG-fMRI-neurofeedback. bioRxiv (2018)
24. Ramoser, H., Mller-gerking, J., Pfurtscheller, G.: Optimal spatial filtering of single trial EEG during imagined hand movement. IEEE Trans. Rehabil. Eng pp. 441–446 (2000)
25. Rosa, M.J., Kilner, J., Blankenburg, F., Josephs, O., Penny, W.: Estimating the transfer function from neuronal activity to BOLD using simultaneous EEG-fMRI. NeuroImage **49**(2), 1496–1509 (Jan 2010)
26. Schwab, S., Koenig, T., Morishima, Y., Dierks, T., Federspiel, A., Jann, K.: Discovering frequency sensitive thalamic nuclei from EEG microstate informed resting state fMRI. NeuroImage **118**, 368–375 (Sep 2015)
27. Sulzer, J., Haller, S., Scharnowski, F., Weiskopf, N., Birbaumer, N., Blefari, M., Bruehl, A., Cohen, L., deCharms, R., Gassert, R., Goebel, R., Herwig, U., LaConte, S., Linden, D., Luft, A., Seifritz, E., Sitaram, R.: Real-time fMRI neurofeedback: Progress and challenges. NeuroImage **76**, 386–399 (Aug 2013)
28. Tagliazucchi, E., Laufs, H.: Multimodal Imaging of Dynamic Functional Connectivity. Frontiers in Neurology **6** (Feb 2015)
29. Thibault, R.T., MacPherson, A., Lifshitz, M., Roth, R.R., Raz, A.: Neurofeedback with fMRI: A critical systematic review. NeuroImage **172**, 786–807 (May 2018)
30. Wang, T., Mantini, D., Gillebert, C.R.: The potential of real-time fMRI neurofeedback for stroke rehabilitation: A systematic review. Cortex (Sep 2017)
31. Zotev, V., Phillips, R., Yuan, H., Misaki, M., Bodurka, J.: Self-regulation of human brain activity using simultaneous real-time fMRI and EEG neurofeedback. NeuroImage **85**, 985–995 (Jan 2014)